

Experimental and Numerical Investigation of Forming Limit Differences in Biaxial and Dome Test

Chetan P. Nikhare

Department of Mechanical Engineering,
Penn State Erie—The Behrend College,
Erie, PA 16563
e-mail: cpn10@psu.edu

For centuries, metals and materials have been characterized using a traditional method called a uniaxial tension test. The data acquired from this test found to be adequate for operations of simple forming where one axis stretching is dominant. Currently, due to the demand of lightweight component production, multiple individual parts eliminated by stamping a single complex shape, which also further reduces many secondary operations. This change is driving by the new fuel-efficiency requirement by corporate average fuel economy of 55.8 miles per gallon by 2025.¹ Due to complex part geometry, this forming method induces multiaxial stress states, which are difficult to predict using conventional tools. Thus, to analyze these multiaxial stress states limiting dome height tests and bulge tests were recommended in many research publications. However, these tests limit the possibilities of applying multiaxial loading and rather a sample geometry changes are required to imply multiaxial stresses. Even this capability is not an option in bulge test due to leakage issue. Thus, a test machine called a biaxial test was devised that would provide the capability to test the specimen in multiaxial stress states by varying the independent load or displacement on two independent axis. In this paper, two processes, limiting dome tests and biaxial tests were experimented, modeled, and compared. For the biaxial tests, a cruciform test specimen was utilized, and conventional forming limit specimens were used for the dome tests. Variation of sample geometry in limiting dome test and variation of loading in biaxial test were utilized to imply multiaxial stress states in order to capture the limit strain from uniaxial to equibiaxial strain mode. In addition, the strain path, forming, and formability investigated and the differences between the tests provided. From the results, it was noted that higher limit strains were acquired in dome tests than in biaxial tests due to contact pressure from the rigid punch. The literature shows that the contact pressure (which occurs when the rigid tool contacts the deformed body), increases the deformation and thus increases the limit strains to failure. This contact pressure parameter is unavailable in biaxial test, and thus, a pure material behavior can be obtained. However, limit strains from biaxial test cannot be considered for a process where rigid tool is processing the metal, and thus, calibration is necessary. [DOI: 10.1115/1.4039587]

Introduction

The demand for light-weight and compact-design vehicles is at the apex of the need for manufacturing due to cost savings as well as continuously growing fuel prices. The need for better fuel performance and crashworthiness in vehicles has grown. The recent changes in economic and environmental regulations are pushing engineers' and researchers' ideas to the limit and forcing them to construct increasingly efficient designs. The struggle lies in how to combine the construction of an efficient design and the requirements for stricter environmental regulations. One way that better design can be created while meeting all the restrictions is to use better materials in construction. An ideal example would use a higher density, high-strength material, and reducing the gage thickness to provide good formability or use a less dense material that somehow lacks in ductility and safe indication in fracture behavior [1]. In both cases, a proper investigation of material

behavior in various deformation modes is necessary to mimic in predictions.

Traditionally uniaxial simple tension tests were dominantly used to characterize the plastic deformation of materials but were found to be insufficient for large strain data while feeding the material, resulting in inaccurate predictions. The reason for this is that the simple uniaxial tension test only provides one mode of deformation, and the data from this test, when used in numerical models, fail to capture other deformation modes and thus need more accurate data-driven models [2]. Uniaxial data lacks to provide enough information on other strain states that are critical to understanding the limitation of the design [3]. It was noted that stresses generated in equibiaxial mode for a particular anisotropy value was much higher than what was found in uniaxial testing [2,4]. In this study, a method called biaxial testing will be numerically simulated for a number of strain states on 5083 aluminum alloy and compared with equivalent hemispherical dome tests by determining the forming limits in each case.

The concept of the forming limit curve (FLC)/forming limit diagram (FLD) on major and minor strain axes was first proposed by Keeler and Backofen [5]. Further on this FLD became one of the useful and powerful tools to analyze a material in various

¹<http://insider.altairhyperworks.com/inspiring-lightweight-design-automotive>

Manuscript received July 28, 2017; final manuscript received February 24, 2018; published online May 28, 2018. Assoc. Editor: Gracious Ngaile.

deformation modes as well as its failure and fracture behavior. This graph uses axes of major and minor strain to plot a failure point for a plane of metal, while it is deformed in various strain states. When these neck points are joined together for strain states from uniaxial to equibiaxial modes, it creates the FLC. This curve provides an indication of how, when and where the material would fail in a particular deformation mode and also provides information that can be used to properly design the die for manufacturing to stop the failure. Strain points above the curve indicate the material failure by necking or tearing and points below refer to the safety of a material [6]. For better viability, the concept has further experimented extensively on various metal grades [7,8]. Further detail studies were performed on the effect of various parameters on this limit curve. It was identified that this limit curve is very sensitive to these parameters: (a) planar and normal anisotropy value “*r*-values” [2,9–12], (b) strain-hardening exponent “*n*-value” [13], (c) temperature [14], (d) strain rate “*e*/*s*-value” [13–15], (e) size of grain at start of deformation [16,17], (f) prestrain [13,17], (g) path dependence [12,18,19], (h) tool geometry [20], (i) in and out of plane forming [21], (j) coefficient of friction between sheet metal and tool which changes the strain path [17], and (k) blank holding force [22]. Traditionally hemispherical dome tests were used to identify the limits of a material in various deformation modes [3]. However, in this method, the punch was in contact with the sheet metal and the deformation plane did not remain on the plane. This contact condition can come in the form of either pressure or friction [23,24]. Friction becomes prevalent simply because the punch is in contact with the sample while manipulating it. This is an unwanted variable that can cause variations in testing and data collection [25–27]. Pressure is the other contact condition that can cause the sample to fail at higher forces or time because of how the pressure makes the material behave while under stress [28–37].

Due to all of the previously mentioned difficulties, a new biaxial test method was developed that can pull the specimen in two directions while varying the pull speeds and generate any number of strain states from uniaxial to equibiaxial modes. A cruciform specimen with a thinner section at the center can be used for this test method where it can provide a uniform strain region when all four arms are pulled in tension. It was observed that the thickness has no influence on the forming limit curve in the biaxial test method [38].

In this paper, forming limit strains were analyzed for specimens tested using the hemispherical dome and biaxial tests. For this purpose, cruciform specimens with a thinner diamond gage at the center were stretched on a biaxial machine to capture different strain paths from uniaxial to equibiaxial strain conditions. Similarly, conventional specimen geometries were considered to evaluate strains from uniaxial to equibiaxial strain condition using hemispherical dome test. In both tests, the failure strain from uniaxial to equibiaxial deformation modes was determined experimentally. Further, the results were compared with thickness gradient criterion (TGC), Marciniak–Kuczynski model, and numerical instability. The differences between limits strains were noted and discussed.

Material

An AA5083 alloy is considered as a part of this study. The material properties were taken from the previously published work by the author [37]. All specimens for the tests were annealed at 500 °C for 5 min to produce softness as the received material showed brittle behavior. Each test was repeated for a set of three specimens in order to establish repeatability. Figure 1 shows the true stress–strain relationship of the uniaxially deformed sample. It can be observed that the material exhibits Luder’s bands. In order to further examine the tensile response of the material, the data were fitted with the power law. The power law fits best from 2.5% to 7.5% strain. The material data that were used for numerical simulation were a combination of actual material data (initial

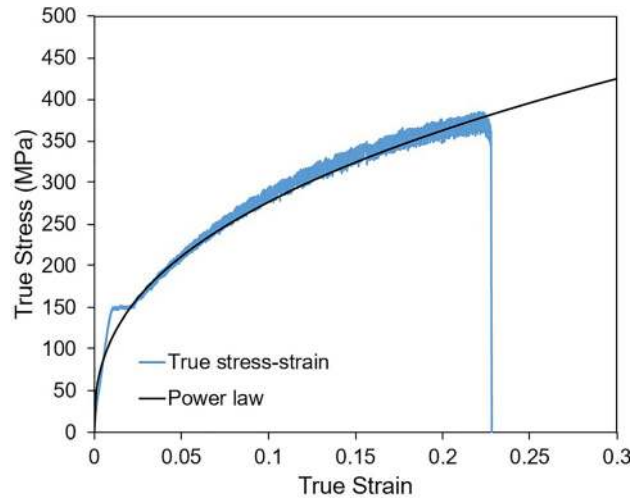


Fig. 1 True stress–true strain curve along with fitted power law (Permission to reprint from ASME @ 2017 [37])

Table 1 Mechanical properties of annealed AA5083 as determined by testing [37]

Engineering yield stress (Mpa)	Engineering tensile stress (Mpa)	Elongation (%)	<i>K</i> (MPa)	<i>n</i>
150	290	26	680	0.39

constant stress for some plastic strain) plus the fitted power law. The mechanical properties characterized from testing are detailed in Table 1, where *K* is the strength coefficient, and *n* is a strain-hardening exponent.

Experimental Methodology

Biaxial Test. Figure 2 shows the cruciform geometry with a diamond-shaped center that was used to perform the tests from uniaxial strain to equibiaxial strain mode on an National Science Foundation-funded biaxial machine. Figure 2 also provides the critical dimensions of a cruciform sample. To produce the maximum deformation at the center, the specimen was milled to a diamond shape from both sides such that the remaining thickness was 0.762 mm. A smooth radius was made in the diamond profile in order to reduce the stress concentration at those locations. From previous studies on the cruciform specimen geometry, it was observed that the recess (gage area) is needed to imply the maximum strain at the center [3], similar to the gage length in the ASTM tensile specimen [39]. With a circular section at the center, it was observed that a more severe stress concentration occurred at the arm intersection corner. Thus, a diamond geometry was chosen, which proved to reduce the stress concentration at the arm intersection and provides a uniform strain gage region. In a previous work by the author [37], digital image correlation (DIC) was used to capture the strain in equibiaxial tests. The tests provided good agreement with the simulation results. To keep consistency between the biaxial tests and dome tests (DIC is difficult to use in current dome testing), 2.54 mm circles were etched (Fig. 2—right image) on the samples to measure the strain at critical regions.

The specimens were then mounted on the biaxial machine such that the two jaws of both of the horizontal and vertical axes were holding the end of each cruciform spoke (Fig. 3). Additionally, the specimens were preloaded with 100 N manually to make sure that there was sufficient contact between the specimen and the jaws. Once confirmed, the horizontal and vertical axes were pulled independently at set conditions (either load or displacement)

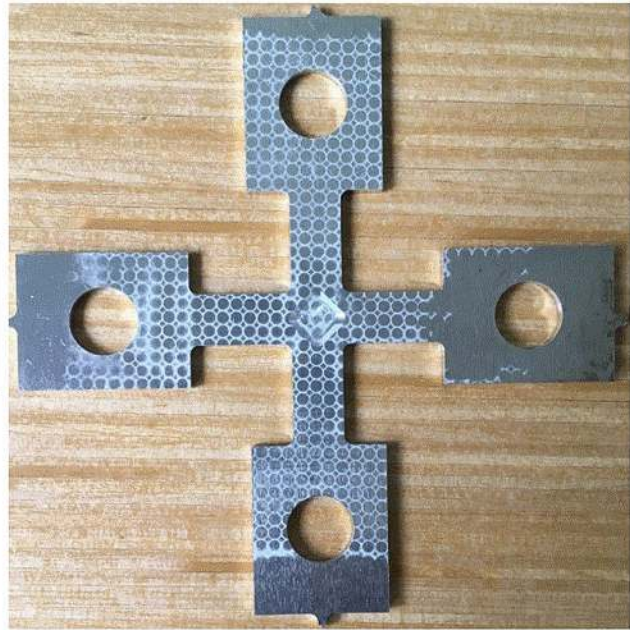
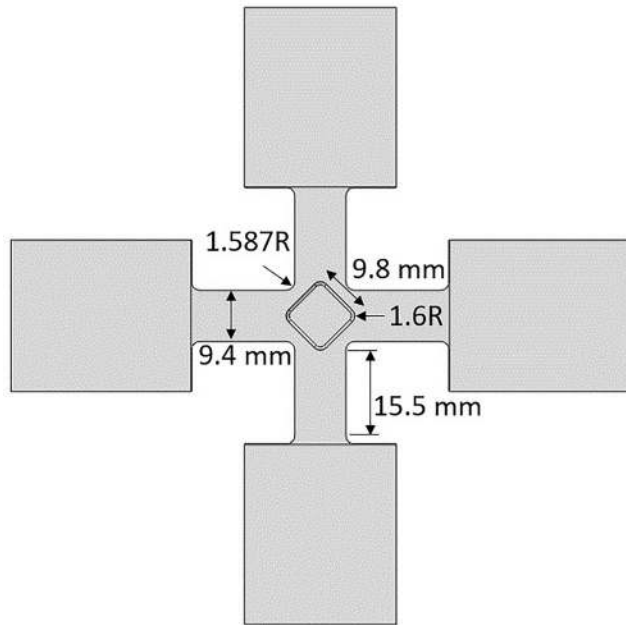


Fig. 2 Cruciform specimen with diamond center

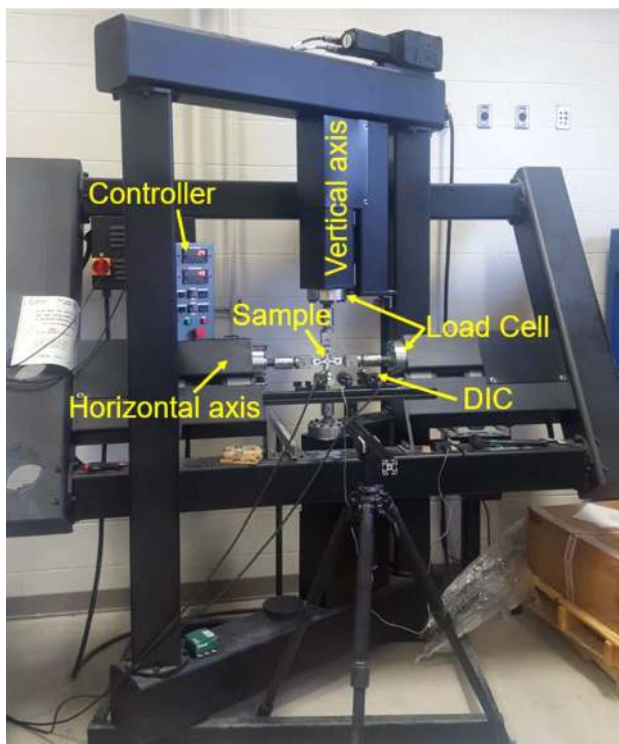


Fig. 3 Biaxial experiment setup with DIC

to provide strains from uniaxial to equibiaxial on the samples. Table 2 provides the experimental pulling speeds on each axis to generate the strain pattern. The machine was manually stopped at the onset of neck/crack. Further, major and minor dimensions of deformed circles were measured and the strains were calculated.

Hemispherical Dome Test

Due to an inability of cruciform specimens to provide the strains in various deformation modes other than only in equibiaxial strain mode in a dome test (previous study [37] by author shows the equibiaxial deformation of cruciform specimen in a dome test by pinching all four spokes between a die and blankholder), conventional samples with varying sizes were used as shown in Fig. 4. As compared to single cruciform dimension specimen, these seven sample geometries are able to provide the strain pattern from uniaxial to equibiaxial strain mode. Due to the nature of the dome test where the movement of hemispherical punch deforms the sheet metal, which is constrained in die and blankholder, a variety of specimen geometries were needed to achieve the strain paths from uniaxial to equibiaxial strain conditions. Similar to the biaxial testing, all specimens were electrochemically etched with 2.54 mm circles (Fig. 5) in order to measure the strain after deformation. Three successful dome tests were conducted for each sample geometry. The Nakajima hemispherical dome test setup is shown in Fig. 6 [40]. The specimen was placed between the die and blankholder and was held in place using tightened bolts. A lock-bead (not shown in the figure) was used to prevent material from feeding inward during the test. The hemispherical punch was set to move with a constant speed of 5 mm/min. To keep the frictionless contact between hemispherical punch and blank, a three-layer sandwich of thin/thick/thin

Table 2 Biaxial test machine axis pulling speed to create a strain pattern

Strain mode	Vertical axis pulling speed (mm/min)	Horizontal axis pulling speed (mm/min)
Uniaxial	5	Free (specimen not mounted on this axis)
Plane-strain	5	0
Between plane and equibiaxial strain	5	2.6
Equibiaxial strain	5	5

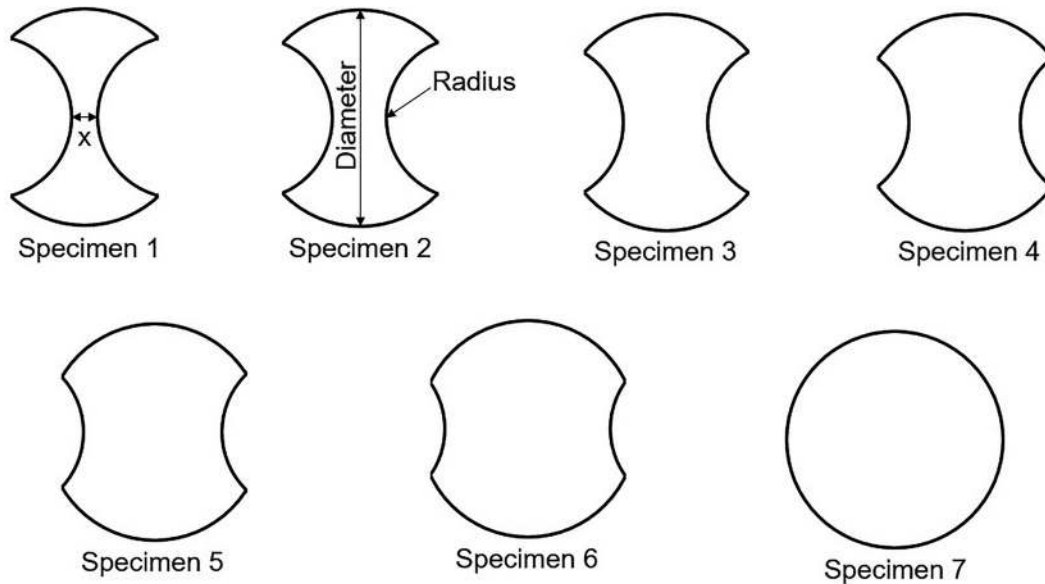


Fig. 4 Seven specimen geometries to provide strain from uniaxial to equibiaxial strain in hemispherical dome test (diameter = 101.6 mm, radius = 38.1 mm, $x = 12.7, 25.4, 38.1, 50.8, 63.5,$ and 76.2 from specimen 1 to 6) [41]

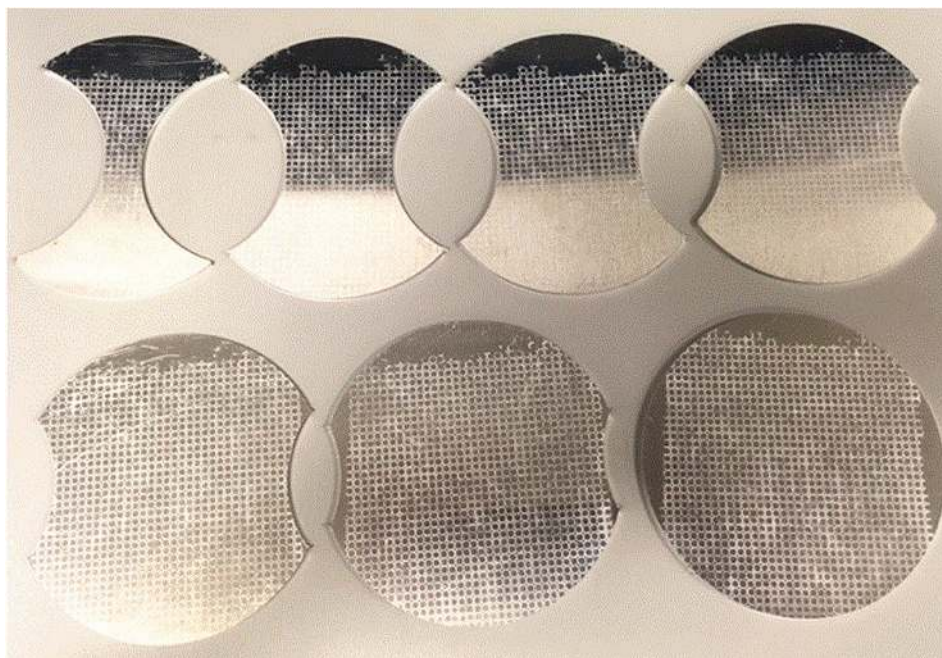


Fig. 5 Electrochemically etched circles on samples

polypropylene was used. In between each layer and between thin polypropylene and blank and punch, a mixture of grease and WD-40 was used. With this method, the failure occurred very near to apex of the dome.

Numerical Methodology

Biaxial Test. ABAQUS/EXPLICIT 6.13-2 was used to simulate all numerical models. To simulate the biaxial tension test on the sample, four outer edges of the sample were constrained to specify the condition. Displacements δ_1 and δ_2 were applied to the end circular arc edges to create various strain paths from uniaxial to biaxial as given in Table 3. A three-dimensional modeling approach was

used to simulate this test (Fig. 7(a)). As measured on the experimental samples, an average representation of thickness on the specimen of 2 mm and 0.762 mm at the center diameter was used [37]. The specimen was kept as a deformable body with S4R shell plane stress elements (four-node quadrilateral, reduced integration). Finer mesh (element size = 0.5 mm) was applied at the center portion of the sample, while the spokes meshed with coarse elements with size = 2 mm (Fig. 7(b)) [37]. Five integration points were used through the thickness to accurately predict the necking. The mesh sensitivity was considered to match the experimental results and is published in the previous work [37]. Three methods were used to predict the neck (a) numerical instability, (b) thickness gradient criterion, and (c) MK model.

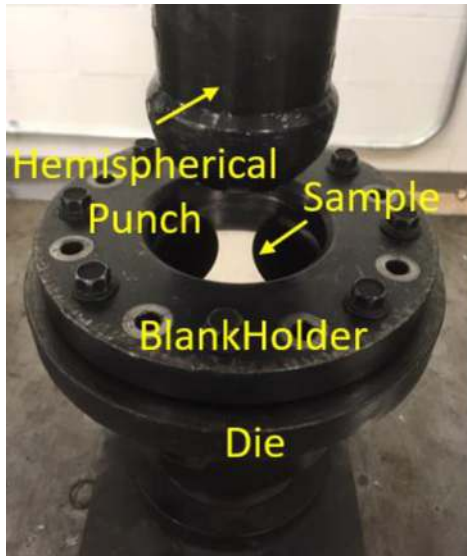


Fig. 6 Nakajima hemispherical dome test setup

Table 3 Displacement of cruciform arm for different strain paths

Sample	δ_1 (mm)	δ_2 (mm)
1	Free	15 (Uniaxial)
2	1.75	15
3	3.5	15
4	9.25	15
5	15	15 (EquiBiaxial)

Dome Test

Similar to the biaxial model, hemispherical dome tests were also simulated using a three-dimensional model approach. The numerical setup is shown in Fig. 8(a). Instead of lock beads, the specimen circumference edge at the lockbead location was constrained as zero displacements. The tooling was assumed as rigid surfaces, while S4R shell elements (four-node quadrilateral, reduced integration) were used to mesh the specimen (Fig. 8(b)). The thickness of the specimen considered was 2 mm, the same as

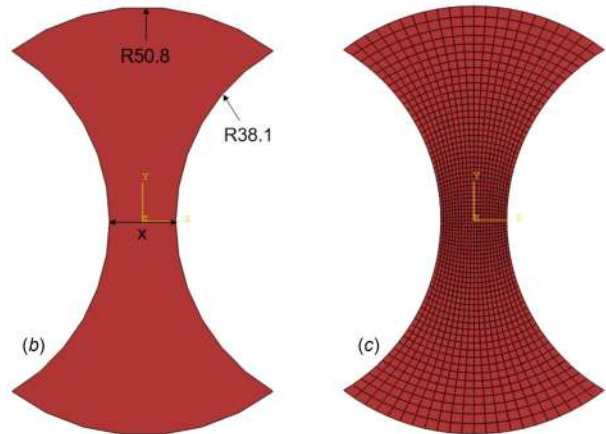
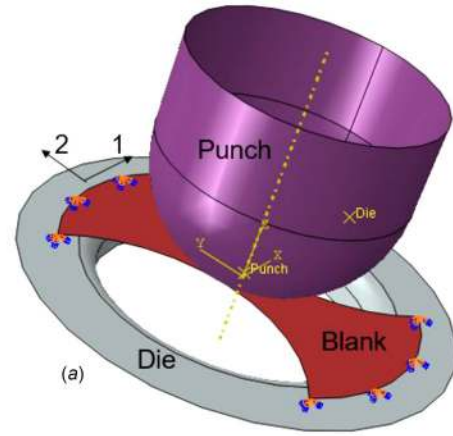


Fig. 8 Nakajima hemispherical dome test (a) numerical model, (b) specimen general dimension, and (c) mesh specimen

measured in experiments. The interaction between the specimen and the tooling was modeled as surface-to-surface contact with no friction, similar to the experiments to avoid the friction effect. To create a strain path spectrum from uniaxial to biaxial strain conditions, different specimen sizes were created as shown in Fig. 8(c) and Table 4. Again, three methods as mentioned earlier were used to predict the neck.

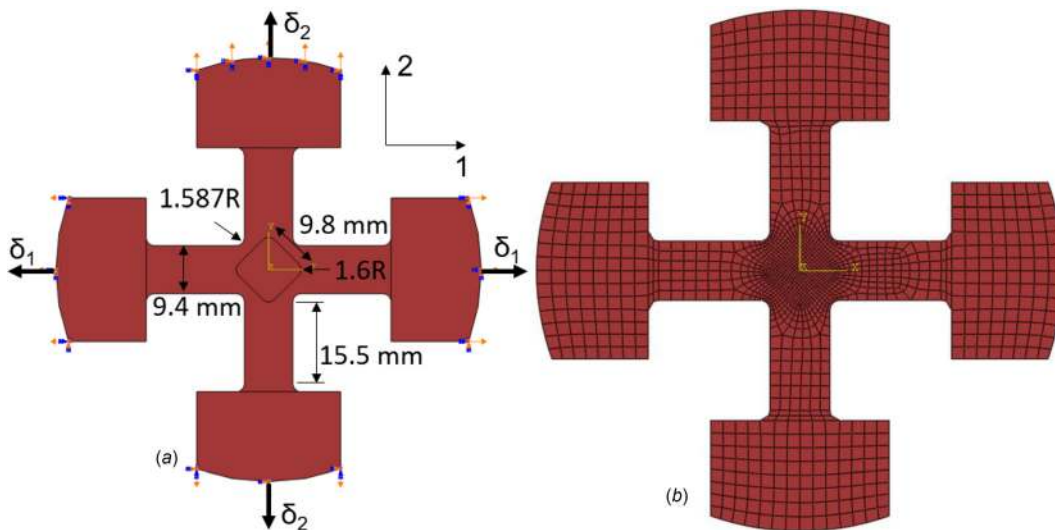


Fig. 7 Cruciform specimen with center diamond (a) with boundary condition and (b) mesh specimen

Table 4 Specimen dimension for different strain paths

Sample	x (mm)
1	12.7 (Uniaxial)
2	38.1
3	50.8
4	63.5
5	101.6 (circular disk) (Equibiaxial)

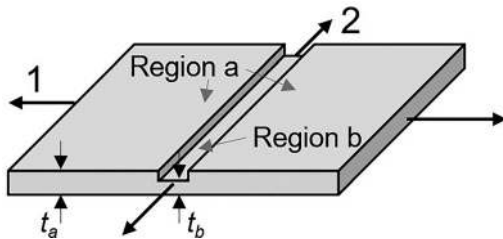


Fig. 9 Schematic illustration of a sheet with pre-existing groove (Reproduced from [49])

Numerical Instability

Numerical instability is based on how the model is setup. Generally, two types of numerical modeling techniques are used: (i) implicit and (ii) explicit. In implicit method, the calculations are based on the previous step known values but also simultaneously depend on the current step and thus have less protection on numerical instability and can lead to diverging solution. In explicit method, the calculations are solely based on the previous step known values, and thus, convergence can be easier in this step [42]. Numerical instability occurs when the load that requires deforming the mesh is continuously dropping [43]. For example, in uniaxial tension, when the force drops, a localized neck can be seen just after the occurrence of the diffuse neck along with a steeper thickness gradient. However, in a biaxial test, a localized neck can be delayed due to uniform deformation of mesh, and a less thickness gradient can be observed, but a diffuse neck might have already occurred, and a force drop would have been noticed. This information can also be seen when the major strain evolution is at a much higher rate than the minor strain [42,44]. This technique is utilized to identify the instability stage, and major and minor strains are plotted in FLD.

Thickness Gradient Criterion

To predict the forming limit strains from numerical simulation, the thickness gradient criterion was used. During sheet metal

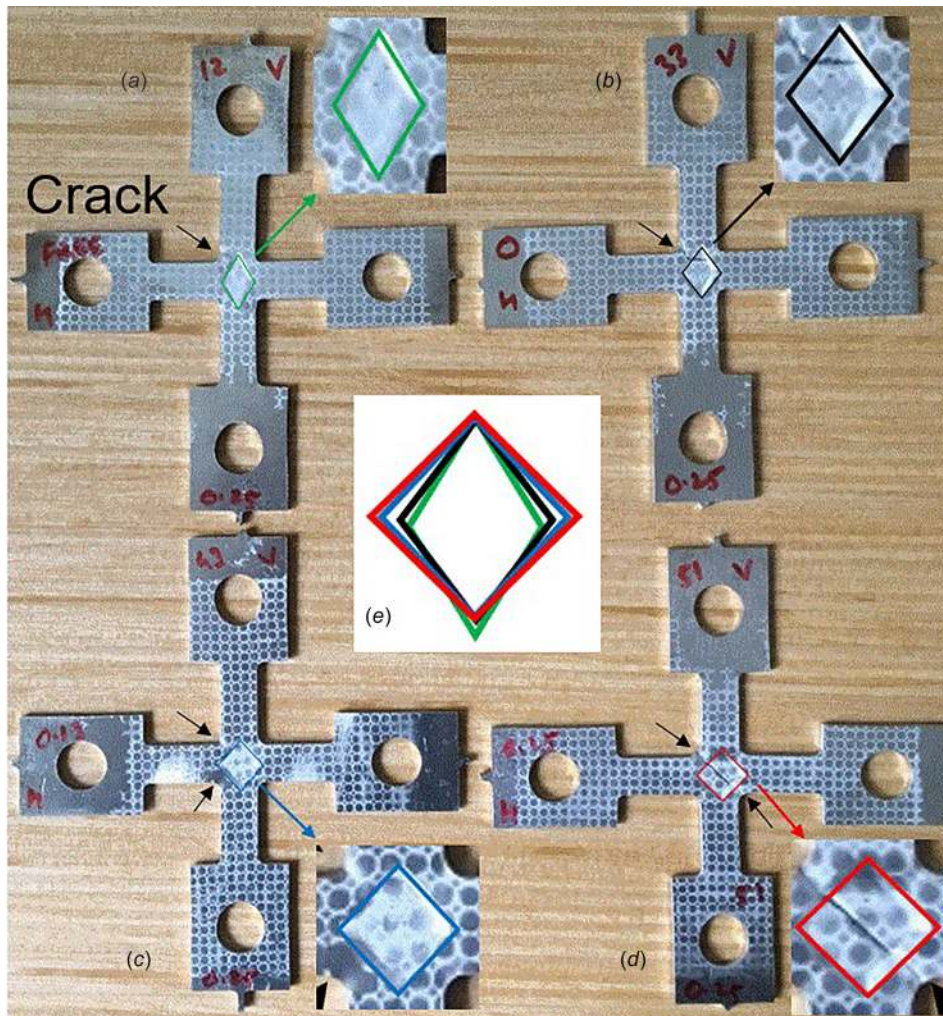


Fig. 10 Deformed samples using biaxial test machine: (a) uniaxial strain, (b) plane-strain, (c) between plane-strain and equibiaxial strain, (d) equibiaxial strain deformation mode, and (e) deformed diamond shape comparison for (a)-(d) deformation modes

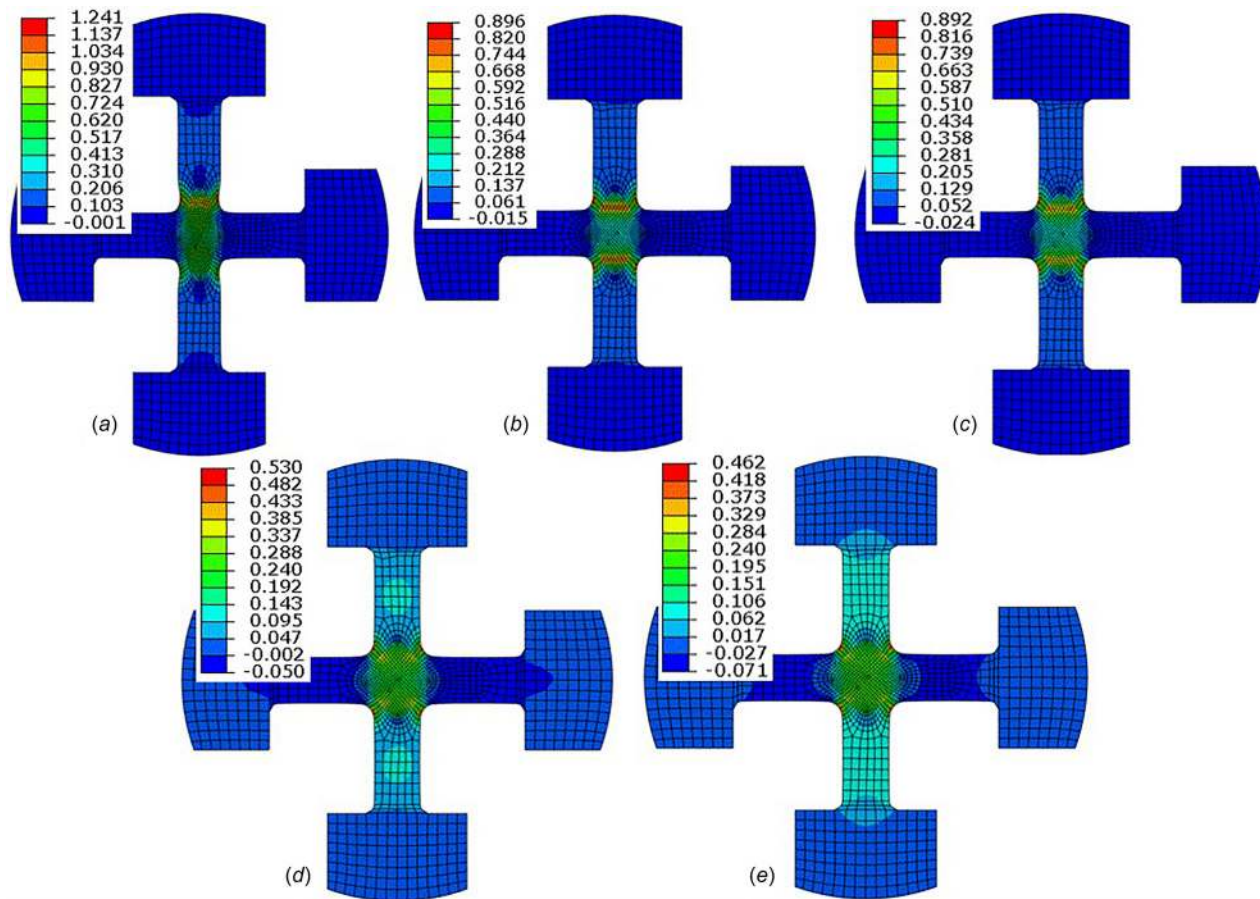


Fig. 11 All formed specimens using biaxial method captured at neck/fail frame: (a) uniaxial strain, (b) between uniaxial strain and plane-strain, (c) plane-strain, (d) between plane-strain and equibiaxial strain, and (e) equibiaxial strain deformation mode (legend shows engineering major strain, i.e., NE22 in ABAQUS)

forming, a localized neck generally occurs, after which the material proceeds to failure. This localized neck is measured/predicted in the form of thickness gradient calculation. Experimentally, it was observed that the localized neck is indicated by the presence of a critical local thickness gradient in the sheet. Such an indication of the neck is independent of the strain path, the rate of forming, and the type of sheet metal (i.e., the material properties) being formed. The critical local thickness gradient, R_c , exists at the onset of a visible local neck. After the start of deformation, a thickness gradient, “ R_{tg} ” develops in the deforming sheet which is expressed in the following equation:

$$R_{tg} = \frac{t_{neck}}{t_{neighbor}} \quad (1)$$

where R_{tg} is the thickness gradient, t_{neck} is the current thickness of a neck element, and $t_{neighbor}$ is the current thickness of a neighboring element.

During forming, this thickness gradient decreases from the initial value of 1.0. The thickness gradient becomes steeper at the onset of localized necking, and at this transition from diffused necking, it attains a critical value. The criterion is represented in the following equation:

$$R_{tg} \leq R_c \quad (2)$$

The R_c is experimentally estimated as 0.92. If R_{tg} is less than 0.92, the component is considered as having necked [45,46].

Marcianiak–Kuczynski Model

The Marcianiak–Kuczynski (MK)-model assumes that an initial defect in the sheet, in the form of a long groove, grows and eventually fails during stretching along the linear strain path in the surrounding material. The pre-existing defect lies perpendicular to the major axis. A sketch of the model is shown in Fig. 9. The 1 and 2 are rolling and transverse directions, and t is the thickness direction. This two-zone material is subjected to plastic deformation, applying a constant incremental stretching of the homogeneous part. When the flow localization occurs in the groove at a critical strain in the homogeneous region, the limiting strain of the sheet is achieved. This criterion of defining the localized neck is provided by Eq. (3). According to this equation, the neck is reached when the increment of major strain in region “b” is equal or greater than ten times the major strain increment in a region “a.” At this state, the values of the major and the minor strain in the homogeneous region are reported for numerical plotting of forming limit diagrams [43,44,47–49].

$$\Delta \varepsilon_{b1} \geq 10 \Delta \varepsilon_{a1} \quad (3)$$

Results and Discussion

Figures 10 and 11 show the deformed samples in uniaxial to biaxial strain conditions. Figures 10(a)–10(d) show samples at fail/neck condition (black arrow directs the failure region). Note that Fig. 10 does not show the test sample between uniaxial strain and plane-strain deformation mode. This is due to the inability to control the machine variability. However, this missing data does

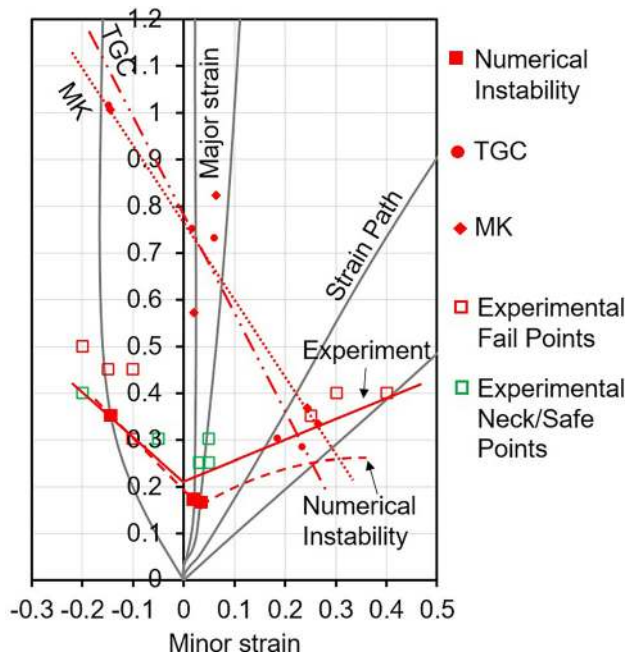


Fig. 12 Forming limit diagram from specimen simulated in biaxial model

not influence the overall conclusion. For an accurate representation, the diamond shapes were placed on the deformed center diamond for an approximate fit. It can be observed that all shapes provide the accurate representation of the deformed shape except for Fig. 10(b). This is because the crack at the corner bent the top vertical arm and thus tilted the top right diamond edge toward the right. If the machine had stopped right at the neck, which is

challenging, the diamond shape would have accurately fit the deformed shape. Furthermore, all these diamond shapes without changing their dimension place on top of each other to present how the diamond evolved from uniaxial to equibiaxial deformation (Fig. 10(e)). The green diamond (uniaxial mode) is dominantly stretch in a vertical direction and compressed in horizontal. When the horizontal direction force increases, the diamond gets a shape toward equisized vertical and horizontal length (refer black, blue, and red diamonds in Fig. 10(e)). Noting the failure, the uniaxial sample (Fig. 10(a)) fails at top vertex of a stretched diamond. The fracture region diverts from diamond vertex to diamond center from uniaxial to equibiaxial sample. Similar observations were made in the numerically deformed samples. Figures 11(a)–11(e) show simulated samples at their critical frame, where the thickness gradient criterion predicted them as in neck condition. Similar predictions were made in terms of the failure region, i.e., the strain element in the uniaxial specimen is near to top arm radius but in the center diamond region (Fig. 11(a)). This neck region continues to divert toward all arm radius as the strain condition changes from uniaxial to a biaxial path and provides uniform strained region at the center diamond for biaxial specimens. In addition, the critical major strain value continues to decrease from uniaxial to a biaxial specimen.

Figure 12 shows the plot of major and minor strains, which is also known as FLD. Failed and necked circle major and minor dimensions were measured, and their strain points were plotted on FLD. The FLC line was plotted such that none of the failed points should be below the line. The plane–strain point is located at 0.215. Further strain paths of a critical element in all five simulated specimens were plotted. These critical elements were selected based on TGC prediction of a necked element in that condition. Additionally, major and minor strains of a thicker neighboring element (safe element) were noted, and red solid circle (for TGC) and red solid diamond (for MK) point were plotted on the FLD to show the limit of a material tested in different directions using the biaxial machine. An approximate line was drawn to



Fig. 13 Seven deformed specimens using dome test: (a) uniaxial strain, (b) and (c) between uniaxial strain and plane–strain, (d) plane–strain, (e) and (f) between plane–strain and equibiaxial strain, and (g) equibiaxial strain deformation mode

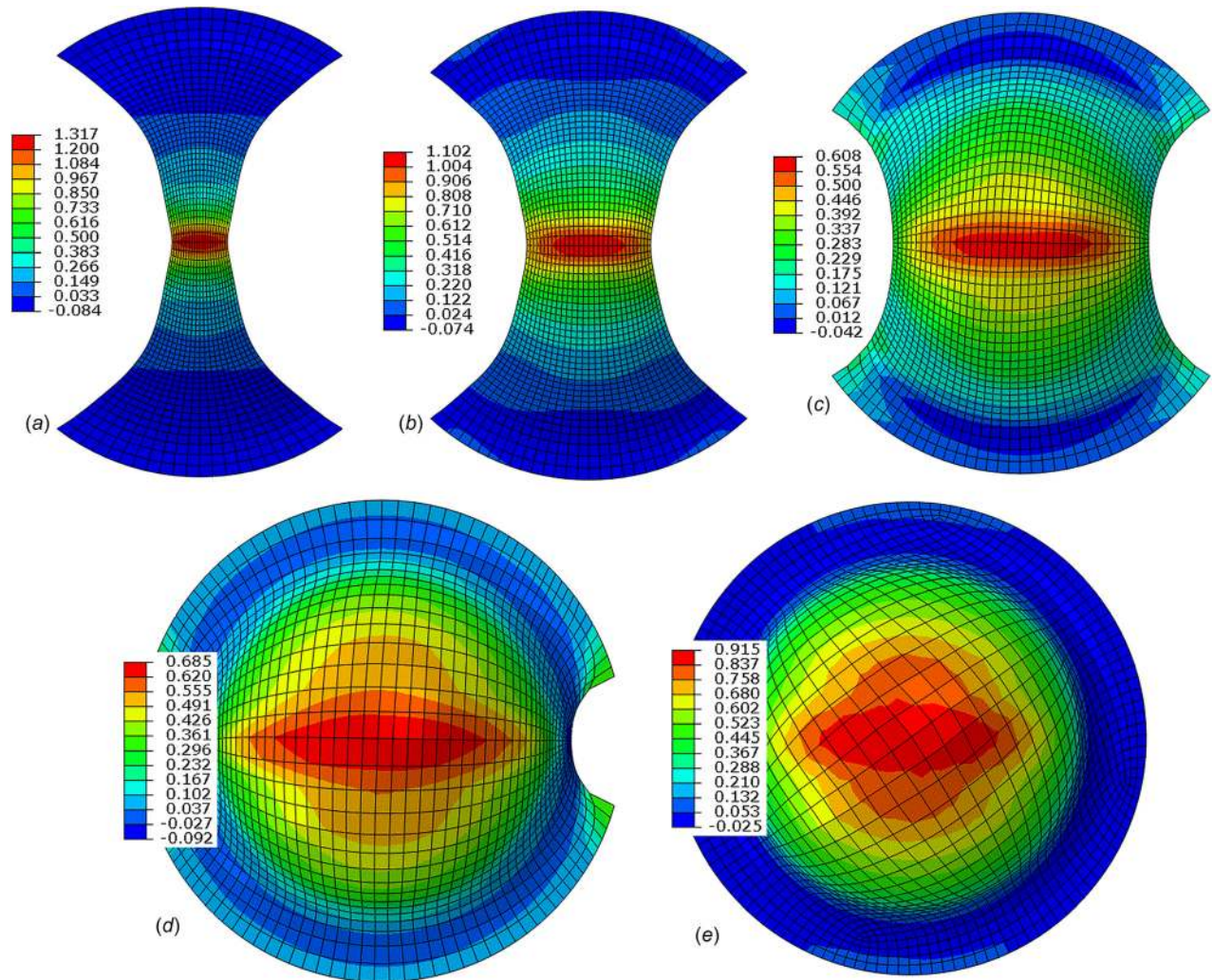


Fig. 14 All formed specimens using dome test method captured at neck/fail frame: (a) uniaxial strain, (b) between uniaxial strain and plane-strain, (c) plane-strain, (d) between plane-strain and equibiaxial strain, and (e) equibiaxial strain deformation mode (legend shows engineering major strain, i.e., NE22 in ABAQUS)

show the limit curve predicted using TGC and MK. TGC and MK models predict the limit strain very close to each other. Upon comparison of the strain path flow with TGC and MK neck prediction during deformation, it was found that the experimental FLC does not match with the TGC and MK prediction. The poor agreement between the experimental data and TGC and MK models is because the criteria were developed using the dome test experiments, where the punch (rigid tool) presses the sheet metal to deform further until failure. However, in the biaxial test machine, no rigid tool contacts the specimen center where it is supposed to fail. Thus, it can be concluded that the conventional failure prediction methods developed using any contact condition would not be able to predict the failure in specimens tested with a biaxial machine.

Additionally, numerical instability points were noted, and red solid square points were plotted. The instability in specimens of uniaxial and near plane-strain paths was realized but not able to capture in a specimen of equibiaxial and near equibiaxial strain paths. Note that due to all spokes of a cruciform specimen being in dominant stretching in equibiaxial strain and near equibiaxial strain mode, numerical instability is hard to achieve. One of the reasons for this is a continuous increase of stress value with respect to strain value in a material curve that was modeled as a power law for the higher amount of strain. Another reason is that the numerical program does not predict the material failure unless

some failure criterion would have been added. A red dashed line was plotted for the limit curve predicted by numerical instability. The numerical instability is in close agreement with the experimental FLC. From the results, it can be concluded that the available analytical methods to predict the forming limit strain that had been developed using testing, where a rigid tool deforms the blank, will overestimate the failure prediction in specimens using a biaxial testing machine.

All seven deformed specimens using dome test are shown in Figs. 13(a)–13(g). Again, the figure shows the sample at fail/neck condition (black arrow indicates the failure region). All five deformed specimens using dome test models are shown in Figs. 14(a)–14(e). The images were captured for all specimens, where TGC predicted the neck/failure. Due to the frictionless condition, all specimens were necked at the near center of the specimen. It can be observed that neck predictions are very closely matched with experiments (match Figs. 13(a) with 14(a), 13(d) with 14(c), and 13(g) with 14(e)). Following a similar procedure, neck/fail circles major and minor dimensions on all specimens were measured and plotted (Fig. 15). Further, a continuous line was drawn such that none of the failure points go below the line, and the FLC was created. As per the conventional forming limit curve, the major strain at failure is highest in the uniaxial specimen, which continuously drops for specimen near plane-strain, and then regains the high major strain when moving toward the equibiaxial

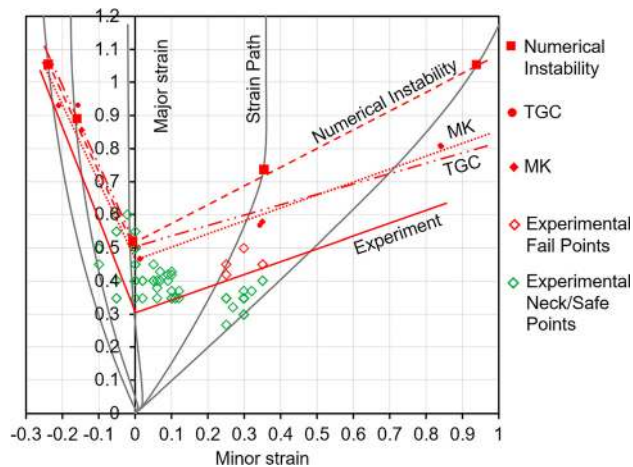


Fig. 15 Forming limit diagram from specimen simulated in dome test model

specimen. The plane-strain point is located at 0.31. Further strain paths of a critical element in all five simulated specimens were plotted. Following the described procedure, these critical elements were selected based on TGC and MK prediction of a neck element in that condition. The major and minor strains of the thicker element were noted and plotted in FLD (solid red circles for TGC and solid red diamonds for MK). Again, an approximate curve is plotted between those points. Also, the numerical instability points were realized and plotted (solid red squares), and the approximate line was drawn. When compared with the numerical instability, it was observed that the MK and TGC prediction lies in very close proximity with the numerical instability, and thus, confirms that the prediction method is viable for failure prediction in a specimen that contacts the rigid tool during deformation. When compared with the experimental FLC, the numerical instability, TGC-, and MK-model provide very close agreement; however, a poor comparison is shown in positive plane-strain. This may be due to the brittleness of AA5083 material, which provides a very little to no neck region in positive plane-strain deformation modes, and the material fails suddenly. This can be observed in the experimentally deformed samples where a small surface material chips during material separation (Figs. 13(d)–13(g)).

The forming limits from all criteria, i.e., TGC, MK-model and numerical instability as well as from experiments in specimens using both methods, i.e., biaxial test and dome test were plotted and compared on FLD. It was observed that with numerical instability the forming limits are much higher in dome tests than biaxial tests. TGC and MK-model were able to predict the failure in dome tests with a close agreement; however, they failed to predict in specimens tested with a biaxial machine. When only the experimental comparison was made between biaxial test and dome test failure, the forming limit strains were higher in dome tests as compared to biaxial tests (Fig. 16).

It was also observed that the plane-strain is 0.1 higher in dome test as compared to biaxial test. This difference is due to the differences in the deformation process. As compared to biaxial tests, in dome tests, the punch contacts the sheet metal and pushes down for deformation; the material is stretched in all axes on sheet plane, but the punch applies contact force through the thickness, and thus, through thickness normal stress influences the fracture mechanics and delays the fracture. This increases the maximum deformation in hemispherical dome tests. Research has shown that application of pressure through the thickness direction changes the thickness plasticity and softens the metals by suppressing the voids [28–37]. Based on the literature, it can be concluded that the difference observed in the two studied process, i.e., biaxial tests where no contact of rigid tool is made in deforming the material, and hemispherical dome tests where a rigid

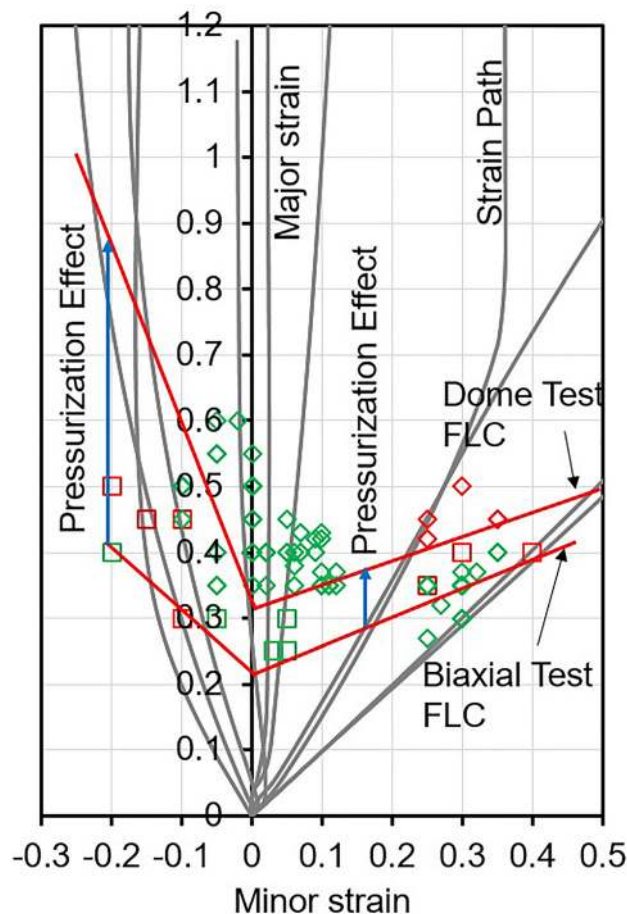


Fig. 16 Forming limit diagram for limit comparison between biaxial test and dome test

punch pushes the metal by applying the contact stress to deform the metal, is due to the pressurization effect. Because of the pressurization effect in hemispherical dome tests, the FLC shifts up as compared to biaxial tests. This shift also depends on how the material behaves in various deformation modes. The FLC might not shift with a constant value due to the change in fracture modes in different deformation modes. This is observed in this study where the difference in the limit strains is higher in uniaxial (i.e., 0.4), but then it decreases with increase in minor strain (i.e., 0.1 in plane-strain and 0.067 in equibiaxial strain). Three findings can be noted: (1) forming limits are higher in dome tests than biaxial tests, (2) the difference (or shift of FLC) might not be same in all deformation modes and is dictated by the failure mode of a particular material in particular deformation mode (for example, it has shown that dual phase steel provides ductile fracture in uniaxial mode but brittle in equibiaxial strain mode [50]), and (3) failure prediction methods developed from dome test, where a rigid tool deforms the specimen, are not applicable for specimens tested with a biaxial testing machine. The reason behind all findings is the pressurization in a specimen during deformation from the rigid tool. Due to the increase in contact pressure from the rigid tool, the forming limits were found to be higher as noted in Refs. [28–37].

Conclusion

This paper discusses the forming limit strains acquired from two testing methods: (a) biaxial tests and (b) dome tests. Experiments were performed on AA5083 annealed material to measure the limit strain in various deformation modes from uniaxial to equibiaxial strain mode. To predict the failure strain and the strain

path of a critical element, both biaxial test, and dome test models were created and simulated in ABAQUS/EXPLICIT 6.13-2. Enough cruciform specimens were utilized to create strain paths from uniaxial to equibiaxial strain conditions by varying the arm displacement. Additionally, conventional circular specimens were considered by changing the gage width in dome tests to result in uniaxial to equibiaxial strain paths. Thickness gradient criterion and the Marciniak–Kuczynski model were used to predict the strain path in both testing methods. In addition, numerical instability was considered to predict the failure. It was observed that the thickness gradient criterion and the Marciniak–Kuczynski model overestimate the failure in the biaxial test method; however, they closely represent the numerical instability in the dome test method. From overall observation, it is concluded that higher limit strains are acquired in dome tests than in biaxial tests due to the contact pressure from the punch. This contact pressure occurs when the rigid tool forces/compresses/contacts the metal during deformation. This pressurization parameter is eliminated in a biaxial test, which is used to characterize the material only and tries to exclude any surrounding effect. It is also concluded that the failure prediction methods developed from the traditional method (i.e., tool forces/contacts and deforms the metal) may not be viable for specimens tested in a biaxial machine.

Acknowledgment

The author would like to thank Penn State Erie, The Behrend College for research facilities and resources and Mr. Glenn Craig for specimen fabrication.

Funding Data

- Directorate for Engineering, National Science Foundation (CMMI No. 1100356).

References

- Mayyas, A., Shen, Q., Mayyas, A., Shan, D., Qattawi, A., and Omar, M., 2011, "Using Quality Function Deployment and Analytical Hierarchy Process for Material Selection of Body-in-White," *Mater. Des.*, **32**(5), pp. 2771–2782.
- Banabic, D., 2016, "Advances in Plastic Anisotropy and Forming Limits in Sheet Metal Forming," *ASME J. Manuf. Sci. Eng.*, **138**(9), p. 090801.
- Abu-Farha, F., Hector, L. G., and Khraisheh, M., 2009, "Cruciform-Shaped Specimens for Elevated Temperature Biaxial Testing of Lightweight Materials," *JOM J. Miner. Met. Mater. Soc.*, **61**(8), pp. 48–56.
- Woodthorpe, J., and Pearce, R., 1970, "Anomalous Behaviour of Aluminum Sheet Under Balanced Biaxial Tension," *Int. J. Mech. Sci.*, **12**(4), pp. 341–347.
- Keeler, S. P., and Backofen, W. A., 1963, "Plastic Instability and Fracture in Sheets Stretched Over Rigid Punches," *ASM Trans. Q.*, **56**(1), pp. 25–48.
- Nikhare, C., Korkolis, Y., and Kinsey, B. L., 2012, "Numerical Analysis of Restrike Process on Al-2008-T4 Aluminum Alloy Square Pan Drawing," International Deep Drawing Research Group Conference, Mumbai, India, Nov. 25–29, pp. 581–686.
- Keeler, S., 1965, "Determination of Forming Limits in Automotive Stampings," *SAE Paper No. 650535*.
- Goodwin, G. M., 1968, "Application of Strain Analysis to Sheet Metal Forming Problems in the Press Shop," *SAE Paper No. 680093*.
- Sowerby, R., and Duncan, J. L., 1971, "Failure in Sheet Metal in Biaxial Tension," *Int. J. Mech. Sci.*, **13**(3), pp. 217–229.
- Arrieux, R., Boivin, M., and Le Maître, F., 1987, "Determination of the Forming Limit Stress Curve for Anisotropic Sheets," *CIRP Ann. Manuf. Technol.*, **36**(1), pp. 195–198.
- Arrieux, R., Bedrin, C., and Boivin, M., 1982, "Determination of an Intrinsic Forming Limit Stress Diagram for Isotropic Metals Sheets," 12th Biennial Congress International Deep Drawing Research Group, Santa Margherita Ligure, Italy, May 24–28, pp. 61–72.
- Da Rocha, A. B., Barlat, F., and Jaliniere, J. M., 1985, "Prediction of the Forming Limit Diagrams of Anisotropic Sheets in Linear and Non-Linear Loading," *Mater. Sci. Eng.*, **68**(2), pp. 151–164.
- Graf, A. F., and Hosford, W. F., 1993, "Calculations of Forming Limit," *Metall. Mater. Trans. A*, **24**(11), pp. 2497–2501.
- Sheng, Z. Q., and Mallick, P. K., 2017, "Predicting Sheet Forming Limit of Aluminum Alloys for Cold and Warm Forming by Developing a Ductile Failure Criterion," *ASME J. Manuf. Sci. Eng.*, **139**(11), p. 111018.
- Ghosh, A. K., 1974, "Strain Localization in the Diffuse Neck in Sheet Metal," *Metall. Trans.*, **5**(7), pp. 1607–1616.
- Stachowicz, F., 1989, "Effects of Microstructure on the Mechanical Properties and Limit Strains in Uniaxial and Biaxial Stretching," *J. Mech. Work. Technol.*, **19**(3), pp. 305–317.
- Li, J., Carsley, J. E., Stoughton, T. B., Hector, L. G., and Hu, S. J., 2013, "Forming Limit Analysis for Two-Stage Forming of 5182-O Aluminum Sheet With Intermediate Annealing," *Int. J. Plast.*, **45**, pp. 21–43.
- Korkolis, Y. P., and Kyriakides, S., 2009, "Path-Dependent Failure of Inflated Aluminum Tubes," *Int. J. Plast.*, **25**(11), pp. 2059–2080.
- Yoshida, K., Kuwabara, T., Narihara, K., and Takahashi, S., 2005, "Experimental Verification of the Path-Independence of Forming Limit Stresses," *Int. J. Form. Process.*, **8**, pp. 283–298.
- Nikhare, C. P., Korkolis, Y. P., and Kinsey, B. L., 2015, "Formability Enhancement in Titanium Tube-Flaring by Manipulating the Deformation Path," *ASME J. Manuf. Sci. Eng.*, **137**(5), p. 051006.
- Raghavan, K. S., 1995, "A Simple Technique to Generate In-Plane Forming Limit Curves and Selected Applications," *Metall. Mater. Trans. A*, **26**(8), pp. 2075–2084.
- Nikhare, C., Filho, R. A. C., Tigrinho, L. M. V., and Marcondes, P. V. P., 2012, "Influence of Blank Holding Force on the Forming Limits of DP590 Steel," International Deep Drawing Research Group Conference, Mumbai, India, Nov. 25–29, pp. 553–559.
- Kuwabara, T., Hashimoto, K., Iizuka, E., and Yoon, J. W., 2011, "Effect of Anisotropic Yield Functions on the Accuracy of Hole Expansion Simulations," *J. Mater. Process. Technol.*, **211**(3), pp. 475–481.
- Ram, S. M., and Kang, H. T., 2010, "Investigation of Hole Expansion Characteristics of DP 600 With Testing and Modeling," *ASME Paper No. IMECE2010-39455*.
- Ko, Y. K., Lee, J. S., Huh, H., Kim, H. K., and Park, S. H., 2007, "Prediction of Fracture in Hub-Hole Expanding Process Using a New Ductile Fracture Criterion," *J. Mater. Process. Technol.*, **187**–**188**, pp. 358–362.
- Narayanasamy, R., Narayanan, C. S., Padmanabhan, P., and Venugopalan, T., 2010, "Effect of Mechanical and Fractographic Properties on Hole Expandability of Various Automobile Steels During Hole Expansion Test," *Int. J. Adv. Manuf. Technol.*, **47**(1–4), pp. 365–380.
- Naka, T., Torikai, G., Hino, R., and Yoshida, F., 2001, "The Effects of Temperature and Forming Speed on the Forming Limit Diagram for Type 5083 Aluminum–Magnesium Alloy Sheet," *J. Mater. Process. Technol.*, **113**(1–3), pp. 648–653.
- Wu, P. D., Embury, J. D., Lloyd, D. J., Huang, Y., and Neale, K. W., 2009, "Effects of Superimposed Hydrostatic Pressure on Sheet Metal Formability," *Int. J. Plast.*, **25**(9), pp. 1711–1725.
- Padwal, S. B., Chaturvedi, R. C., and Rao, U. S., 1992, "Influence of Superimposed Hydrostatic Tension on Void Growth in the Neck of a Metal Sheet in Biaxial Stress Fields—Part II: Plastic Instability," *J. Mater. Process. Technol.*, **32**(1–2), pp. 99–107.
- Banabic, D., and Soare, S., 2008, "On the Effect of the Normal Pressure Upon the Forming Limit Strains," Seventh International Conference and Workshop on Numerical Simulation of 3D Metal Forming Process (Numisheet), Interlaken, Switzerland, Sept. 1–5, pp. 1–5.
- Allwood, J. M., and Shouler, D. R., 2009, "Generalised Forming Limit Diagrams Showing Increased Forming Limits With Non-Planar Stress States," *Int. J. Plast.*, **25**(7), pp. 1207–1230.
- Zhang, F., Chen, J., Chen, J., and Zhu, X., 2014, "Forming Limit Model Evaluation for Anisotropic Sheet Metals Under Through-Thickness Normal Stress," *Int. J. Mech. Sci.*, **89**, pp. 40–46.
- Zhang, F., Chen, J., and Chen, J., 2014, "Effect of Through-Thickness Normal Stress on Forming Limits Under Yld2003 Yield Criterion and MK Model," *Int. J. Mech. Sci.*, **89**, pp. 92–100.
- Nurcheshmeh, M., and Green, D. E., 2014, "The Effect of Normal Stress on the Formability of Sheet Metals Under Non-Proportional Loading," *Int. J. Mech. Sci.*, **82**, pp. 131–139.
- Wang, H., Wu, P. D., Lee, S. Y., Wang, J., and Neale, K. W., 2015, "Numerical Study of the Effects of Shear Deformation and Superimposed Hydrostatic Pressure on the Formability of AZ31B Sheet at Room Temperature," *Int. J. Mech. Sci.*, **92**, pp. 70–79.
- Banabic, D. ed., 2016, *Multiscale Modelling in Sheet Metal Forming*, Springer, Berlin.
- Nikhare, C. P., Vorisek, E., Nolan, J., and Roth, J. T., 2017, "Forming Limit Differences in Hemispherical Dome and Biaxial Test During Equi-Biaxial Tension on Cruciform," *ASME J. Eng. Mater. Technol.*, **139**(4), p. 041011.
- Nikhare, C. P., 2018, "Numerical Analysis on the Effect of Thickness on Biaxial Tension Limits," *Mater. Today: Proc.*, **5**(1), pp. 37–43.
- ASTM, 2004, "Standard Test Methods for Tension Testing of Metallic Materials," ASTM International, West Conshohocken, PA, Standard No. *ASTM E8-04*.
- Nakazima, K., Kikuma, T., and Hasuka, K., 1968, "Study on the Formability of Steel Sheets," *Yawata Tech. Rep.*, **264**, pp. 8517–8530.
- Abu-Farha, F., 2011, "The Development of a Forming Limit Surface for 5083 Aluminum Alloy Sheet," *JOM*, **63**(11), pp. 72–78.
- Menezes, L. F., and Teodosiu, C., 2000, "Three-Dimensional Numerical Simulation of the Deep-Drawing Process Using Solid Finite Elements," *J. Mater. Process. Technol.*, **97**(1–3), pp. 100–106.
- Wagoner, R. H., and Chenot, J. L., 2001, *Metal Forming Analysis*, Cambridge University Press, Cambridge, UK, pp. 198–199.
- Hasan, R., Kasikci, T., Tsukrov, I., and Kinsey, B. L., 2014, "Numerical and Experimental Investigations of Key Assumptions in Analytical Failure Models for Sheet Metal Forming," *ASME J. Manuf. Sci. Eng.*, **136**(1), p. 011013.

- [45] Kumar, S., Date, P. P., and Narasimhan, K., 1994, "A New Criterion to Predict Necking Failure Under Biaxial Stretching," *J. Mater. Process. Technol.*, **45**(1–4), pp. 583–588.
- [46] Nandedkar, V. M., 2000, "Formability Studies on a Deep Drawing Quality Steel," Ph.D. thesis, IIT Bombay, Mumbai, India.
- [47] Marziniak, Z., and Kuczynski, K., 1967, "Limit Strain in the Process of Stretch-Forming Sheet Metals," *Int. J. Mech. Sci.*, **9**(9), pp. 609–620.
- [48] He, J., Xia, Z. C., Li, S., and Zeng, D., 2013, "M–K Analysis of Forming Limit Diagram Under Stretch-Bending," *ASME J. Manuf. Sci. Eng.*, **135**(4), p. 041017.
- [49] Hosford, W. F., and Caddell, R. M., 1993, *Forming Limits. Metal Forming-Mechanics and Metallurgy*, 2nd ed., Prentice Hall, Upper Saddle River, NJ.
- [50] Nikhare, C., Hodgson, P. D., and Weiss, M., 2011, "Necking and Fracture of Advanced High Strength Steels," *Mater. Sci. Eng. A*, **528**(6), pp. 3010–3013.